Jurnal Teknologi Reaktor Nuklir

Tri Dasa Mega

Journal homepage: jurnal.batan.go.id/index.php/tridam

Strain Analysis of Reactor Type Core Structures by Considering Uncertainties of Graphite's Properties

Mike Susmikanti[1*], Roziq Himawan[2], Jos Budi Sulistyo[3], Farisy Yogatama Sulistyo[1].

[1]*Center for Nuclear Reactor Technology and Safety (PTKRN Batan), Kawasan Puspiptek, Tangerang Selatan, 15310, Indonesia*
[2]*Center for Informatics and Nuclear Strategic Zona Utilization (PPIKSN Batan), Kawasan Puspiptek, Tangerang Selatan, 15310, Indonesia*
[3]*Center for Nuclear Facilities Engineering (PRFN Batan), Kawasan Puspiptek, Tangerang Selatan, 15310, Indonesia*

ARTICLE INFO

Article history:

Received: 26 December 2020
Received in revised form: 28 January 2021
Accepted: 5 February 2021

Keywords:

Strain Analysis
HTGR
Graphite IG-110
Probabilistic Analysis

A B S T R A C T

The power reactor with high-temperature gas-cooled reactor (HTGR) technology uses uranium as the reactor fuel. The energy from fission is converted to electrical energy or used for other needs such as hydrogen production or other research activities at high temperatures of around 700 °C. This operation does not allow the use of metal as the core material for the reactor. The material that fits the requirements as a core structure is graphite. Graphite material has specific characteristics, namely the parameters of the modulus of elasticity, coefficient of thermal expansion, and the volume which changes due to temperature and neutron dose. Because the structure of the reactor core is a vital component in the reactor, this research will develop a method for the design of the reactor core structure with graphite material. The design method is based on "Design by Analysis" which specifically refers to the strain analysis on each of the reactor core components. The design method developed is based on the finite element method. The object of this research is the side reflector made from the Toyo Tanso IG-110 series graphite. Based on the analysis of heat distribution and heat stress for the material before the effect of neutron exposure, the temperature distribution on the side reflector was found, as well as the displacement and heat stress that occurs isotropic properties, Young's modulus and Poisson's ratio values can be verified and estimated. The purpose of this research is to analyze the strain of the reactor core structure by taking into account the uncertainty of the graphite properties.

1. INTRODUCTION

The High temperature gas cooled reactor (HTGR) was chosen because of its inherent safety characteristics, it will automatically extinguish any uncontrolled reactions. Unlike the light water-cooled reactor types, the pressurized water reactor (PWR) and the boiling water reactor (BWR), the HTGR is designed to operate at a high temperature of 700 ^{0}C as shown in Figure 1. In addition to its safety characteristics, the HTGR has another advantage in that it can be used in cogeneration by utilizing residual heat from steam generation.

*Corresponding author. Tel./Fax.:021 756 0912/756 0913
E-mail: mike@batan.go.id
DOI: 10.17146/tdm.2021.23.1.6172

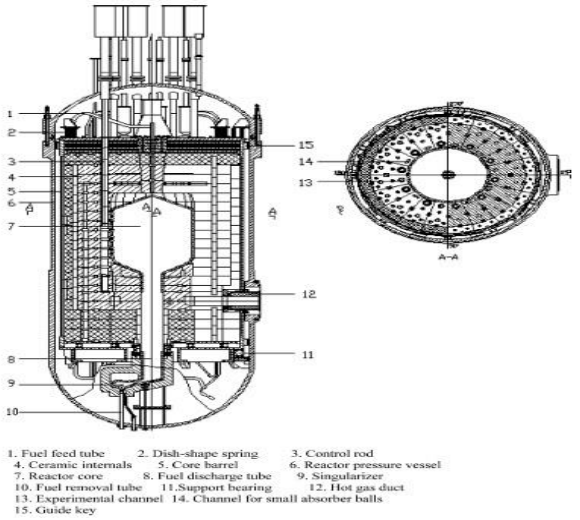

Fig. 1. Design of HTGR-type reactor core

In the HTGR, Graphite is chosen as the main core structural material to replace metal materials. Graphite is the main material for the HTGR-type reactor core. As a reference for designing HTGR type reactor core, requirements or design criteria have been formulated[1]. Based on these requirements, a graphite material was developed for use in the manufacture of HTGR reactor cores. In the development process, the characterization of the graphite material mechanical properties such as tensile strength, fatigue and creep behavior has been carried out[2]. At high temperatures, the creep phenomenon is a very dominant trigger for the degradation of the graphite material. In addition, the neutron irradiation factor will have a worse impact on the creep phenomenon. Therefore, to anticipate all aspects of the triggers for the degradation of the graphite material, a design method was developed especially considering the neutron irradiation factor and the creep phenomenon on the reflector component.

At the analysis stage, the actual test results have been verified with the conditions of graphite material at the time the installation was operating [3–5]. In the reflector specimen compression test, the amount of strain that occurs in the specimen has been actually measured. Furthermore, this value has been compared with the results of the analysis by simulation [6, 7]. Based on previous research, non-destructive testing methods and deterministic methods have been carried out on graphite [8–10].

Likewise, probabilistic reliability analysis and articial-intelegence-based have been carried out in terms of fracture mechanics for the Reactor Pressure Vessel [11, 12]. A probabilistic stress distribution analysis in thick cylindrical pipe and a probability study on thermal Stress in thick HK40 stainless steel pipe has been carried out using finite element method [13–15].

Analysis of the HTGR type reactor core design using graphite material includes the method of testing the graphite material and design evaluation. In evaluating the reactor design, a component stress analysis is carried out and the results are compared with the criteria established by the Code and Standard.

Until now, the design method based on probabilistic reliability analysis has not been developed far enough to anticipate the uncertainty of the mechanical properties of the IG-110 graphite material.

This study aims to develop a design method that includes the mechanical testing method of IG-110 graphite material and probabilistic strain analysis of IG-110 graphite based on finite element method. This research focuses on the prediction of mechanical properties, prediction of stress and the results of the study of changes in the properties of IG-110 due to neutron exposure. Strain analysis based on the finite element method was carried out after a probabilistic approach is carried out.

In testing the material properties, the experimental data were fitted. The fitting stages are: regression modeling, data interpolation which resulted in the distribution of data around the temperature of 700^0C, probabilistic goodness of fit testing and estimation of distribution parameters. Afterward, using the appropriate probability distribution and its distribution parameters, a simple random sampling simulation was carried out. Then, the simulation results are used in the simulation of stress and strain analysis of mechanical components. This research is expected to provide benefits in the analysis of the design of the reactor core structure, especially those made of IG-110 graphite material.

2. THEORY

The HTGR type reactor core reflector is shown in Figure 2.

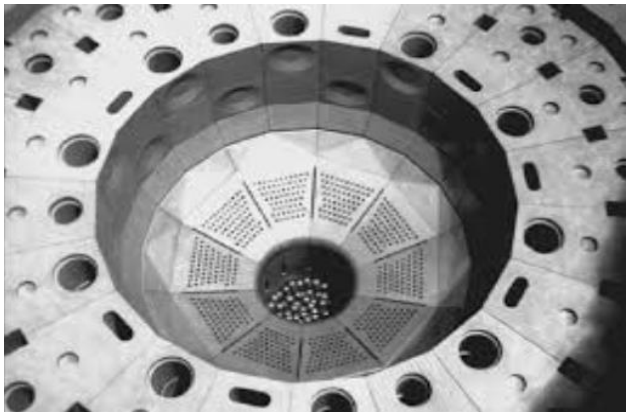

Fig. 2. HTGR core reflector

The surface of the reflector that is subjected to pressure, temperature, and neutron exposure is shown in Figure 3.

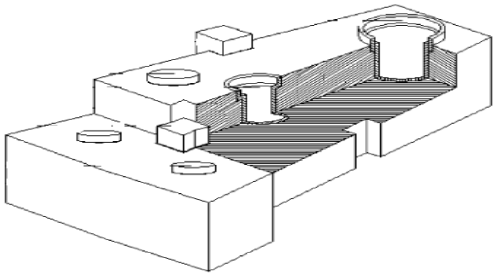

Fig. 3. Reflector surface

The miniature specimen of the reflector component is shown in Figure 4.

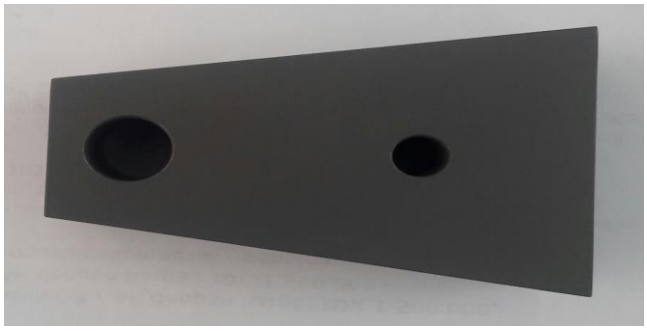

Fig. 4. Miniature specimen of the reflector component

In simulating radial load of graphite IG-110 un-irradiated and irradiated, it is necessary to define the compressive load, the model boundary parameters, and the mechanical properties of graphite. The mechanical properties of IG-110 are shown in Table 1[1].

Table 1. Mechanical Properties of IG-110

Density (g/cm^3)	1.76
Modulus Elasticity (GPa)	9.04
Tensile Strength (MPa)	25.40
Compress Strength (MPa)	76.22
Poisson ratio	0.126
Friction Coefficient	0.369

Radiation exposure or fluence is the radiant energy received by the surface area of the unit, or the equivalent of surface irradiation, integrated from the irradiation time with units (J/m^2). Based on the research results, the modulus of elasticity E is influenced by the fluency of neutron Φ, namely the cumulative number of neutrons passing through a unit area of a material during a specified duration.

There are two compressive loads received by the graphite. The first load arises from the graphite pile on top and the second load comes from the radial strain (length increase) compressive load due to fluence and/or temperature changes. The mass is expressed in Eq. (1)

$$m = \rho.V \quad (1)$$

In (1), m is mass (kg), ρ is density and V is volume. Weight is the product of mass and gravity. The compressive load due to the pile is calculated from the total weight of the graphite pile as expressed in Eq. (2).

$$W = \sum m.g \quad (2)$$

Here, W is the compressive load due to the pile's weight, m is the mass of one graphite component and g is the gravity of the earth (9.81 m/s^2).

In Figure 5, there are four components of the graphite top reflector and ten components of the graphite side reflector which stack on top of the simulation model.

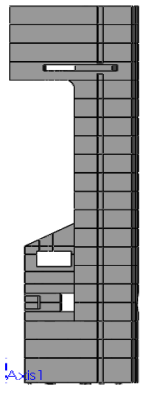

Fig. 5. Internal cutting of the ceramics reflector for the top and bottom sides

The calculation of the vertical load received by the model can be seen in Table 2.

Table 2. Estimation of compressive load by graphite mass

Type of Reflector	Volume (cm^3)	Mass (kg)	Load (N)	Total Load (N)
Top Reflector	125524.27	220.92	2167.26	8669.02
Side Reflector	85646.70	150.74	1478.74	14787.40

The compressive load is due to the 3-MPa operating pressure of the HTR. This value will be used as the compressive load on the front of the graphite.

In the safety analysis, when graphite receives neutron irradiation, its strain will initially decrease; however, it will increase as the fluence increase beyond the certain value. The limit value of increasing strain is used as a reference value for the safety criteria for graphite. The pressure load due to this strain is calculated with Eq. (3)[1, 15],

$$E = \frac{\sigma}{e} \quad (3)$$

In Eq. (3), E is the modulus of elasticity of graphite, σ is the stress and e is the strain. So that the working load is obtained as stated in Eq. (4)[1, 15],

$$\sigma = E.e \quad (4)$$

The values obtained will be used as radial load in the simulation model.

During operation, reflector components in the HTGR core will receive various stressors or aging triggers such as forces / stresses, temperature and neutron exposure. Any one type of aging trigger will result in strain on the reflector components. Due to the present of various triggers, various strain can occur depending on the triggers. In carrying out an analysis of the integrity or reliability of the reflector component, ideally, it should take into account any strain caused by these triggers. The total strain that occurs in the reflector component is expressed in Eq. (5)[15],

$$\varepsilon_{Total} = \varepsilon_{Elastis} + \varepsilon_{Thermal} + \varepsilon_{Irradiation} \quad (5)$$

where

$\varepsilon_{Elastis}$: strain caused by forces/stresses with the main parameters E (Young's modulus) and ν (Poisson's ratio)

$\varepsilon_{Thermal}$: strain caused by temperature differences with parameters E (Young's modulus), ν (Poisson's ratio), and α (thermal expansion coefficient)

$\varepsilon_{Irradiation}$: strain caused by irradiation with parameters E (Young's modulus) and ν (Poisson's r*atio)*

Strain analysis was performed using finite element method. Strain analysis can be used to verify a reactor design that takes into account the effects of neutron radiation exposure. The graphite material in the reflector component occurs due to neutron exposure, mechanical loads, temperature differences that trigger heat stress, and strain due to the creep phenomenon.

For the goodness-of-fit test, the data of the Young's modulus and the change in the dimensions of the graphite material are assumed to follow either Weibull, lognormal, normal, or exponential distribution[16]. The exponential probability distribution has a probability density function (pdf) as expressed in Eq. (6)[16],

$$f(x) = \lambda \exp(-\lambda x),\ x>0 \quad (6)$$

The expected value, *E(x)* for the exponential distribution is expressed in Eq. (7)[16],

$$E(x) = \frac{1}{\lambda} \quad (7)$$

The pdf of Weibull distribution is expressed in Eq. (8)[16],

$$f(x) = \frac{\beta}{\eta}(\frac{x}{\eta})^{\beta-1} \exp[-(\frac{x}{\eta})^{\beta}]\ x>0, \eta, \beta \geq 0 \quad (8)$$

The average value *E(x)* for the Weilbull distribution is given by Eq. (9) [16],

$$E(x) = \eta x\ \Gamma(\frac{1}{\beta}+1] \quad (9)$$

The pdf of the normal distribution is expressed in Eq. (10)[16],

$$f(x) = \frac{1}{\sigma\sqrt{2\pi}} \exp(-\frac{1}{2})(\frac{t-\mu}{\sigma})^2),\ x>0, \eta, \beta \geq 0 \quad (10)$$

Eq. (11) gives the average of the normal distribution,

$$E(x) = \eta \quad (11)$$

The pdf of lognormal distribution is expressed in Eq. (12) [16],

$$f(x) = \frac{1}{x\sigma\sqrt{2\pi}} \exp(-\frac{1}{2})(\frac{\ln t - \mu_x}{\sigma_x})^2) \quad (12)$$

Its average value is expressed in Eq. (13)[16].

$$E(x) = \eta \quad (13)$$

Simple Random Sampling (SRS) simulation were performed to generate the sample value of the variable (X_{1i}, X_{2i}, ⋯ X_{ni}). The variable X_i are the modulus young and dimensional change by generating random numbers, and calculating the value of Y_i according to the density function and characteristic parameters. Sampling on the input variable X = (x_1, x_2, .., x_n) to produce a sample that represents the cumulative distribution function of the input variable [11, 14]. Furthermore, the variable Z (z_1, z_2, .., z_n), is the transformed variable where n is the number of samples, given, into the values of the random variable X_i following the given distribution. Simple transformation is an

inverse transformation method. Where is the inverse of cumulative distribution function of random variable X [11, 14]. The probabilistic analysis using the SRS method is expected to anticipate the uncertainty of the graphite material properties[17].

3. METHODOLOGY

Based on models of creep strain for graphite material at HTGR and JAERI reference[1], experiments were carried out for determination of the Young's modulus *E* at the room temperature of 20 °C, followed by further experiments at temperatures of 400 °C, 600 °C, 800 °C, 1000 °C, and 1200 °C. Afterward, the results of the experiments at those elevated temperatures were compared with the results from room temperature. Thus, Engauge Digitizer's fitting ability can be used to interpolate to temperatures around 700 °C, which is within the range of 600 °C to 800 °C. The fitting of E/E_0, the Young's modulus normalized to its value at 20 °C, was performed at 400 °C to 1200 °C. A suitable regression model was created for the normalized Young's modulus E/E_0. Then, the interpolation was carried out at temperatures ranging from 600 °C to 800 °C.

The goodness-of-fit test was carried out for the appropriate distribution using the MINITAB software. The distributions considered were Weibull, normal, lognormal and exponential distributions. As a result, the distribution parameters are obtained. Those parameters were subsequently used in the SRS simulation to obtain E/E_0 value at around 700 °C.

In the same way, the E/E_0 fitting was performed based on experimental data at temperatures of 400 °C, 600 °C, 800 °C, 1000 °C, and 1200 °C for neutron fluences of 0, 1, 2, 3, 4, 5, and 6 zetta-neutrons (Zn, 10^{21} neutrons) per square-centimeter. The goodness-of-fit test was carried out to find the suitable dispersion parameters. A total of n = 25 random numbers were chosen to generate the E/E_0 random number by simulating the SRS for fluences of 0, 1, 2, 3, 4, 5, and 6 Zn/cm^2 respectively, with the appropriate distribution parameters provided.

Calculation of the dimensional changes at temperatures of 600 °C to 800 °C for fluences of 0 to 6 Zn/cm^2 followed the same steps as Young's modulus calculations. Furthermore, the Young's modulus and dimensional change values obtained from SRS simulations were substituted into a simulation of strain analysis calculations using SolidWorks software package using finite element method.

4. RESULTS AND DISCUSSION

Fitting was performed to obtain E/E_0 according to reference data in Figure 6[1] using Engauge Digitizer software package at temperatures of 200 °C to 1600 °C.

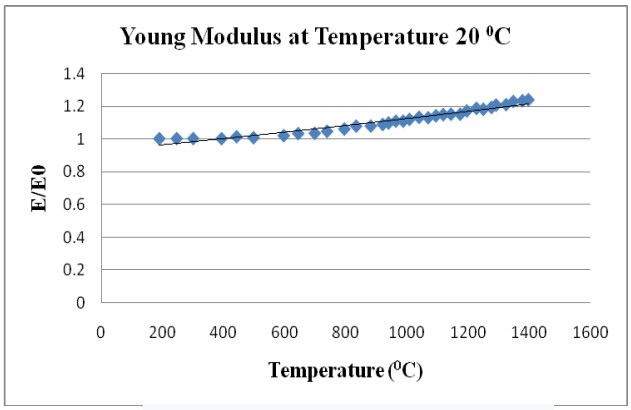

Fig. 6. Normalized Young's modulus E/E_0 at room temperature 20 °C

Afterward, a regression model was created for E/E_0 at a temperature of 200 °C to 1600 °C against room temperature of 20 °C, as in Figure 7.

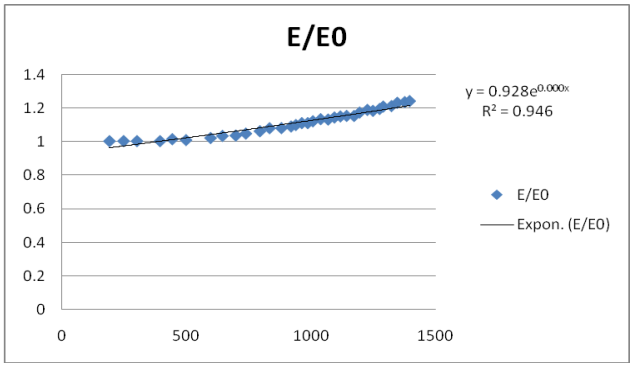

Fig. 7. Young's modulus E/ Eo regression model

Interpolation was carried out for the E/E_0 modulus at a temperature of 600 °C to 800 °C as shown in Table 3.

Table 3. The results of the interpolation of modulus young E / E_0 at temperatures of 600 °C to 800 °C

Temp	E/Eo	E
600	0.9732	8.2240
610	0.9727	8.2351
620	0.9722	8.2464
630	0.9718	8.2579
650	0.9708	8.2815
665	0.9700	8.2997
680	0.9693	8.3184
700	0.9683	8.3440
725	0.9670	8.3771
740	0.9663	8.3976
750	0.9658	8.4115
765	0.9651	8.4327
775	0.9646	8.4471
790	0.9638	8.4691
800	0.9633	8.4840

From the distribution suitability test (Figure 8) the probability density function was obtained for Weibull distribution.

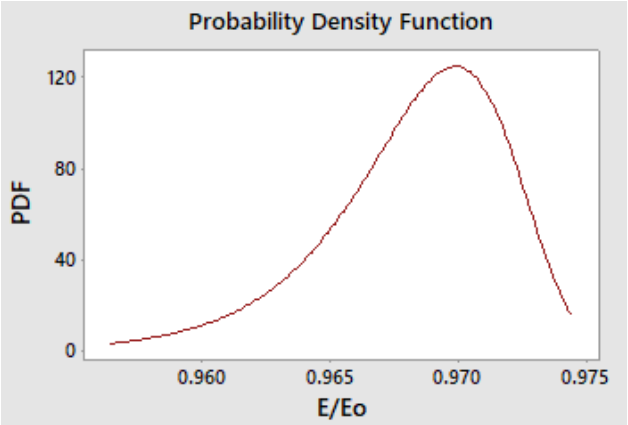

Fig. 8. Suitability test and Weibull distribution parameters

The probability distribution and the parameters shape and scale of Weibull are shown in Figure 9

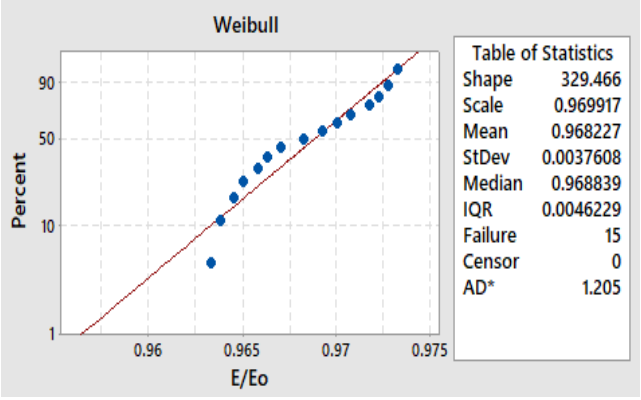

Fig. 9. The probability of Weibull Distribution

Afterward, generate the SRS as shown in Figure 10.

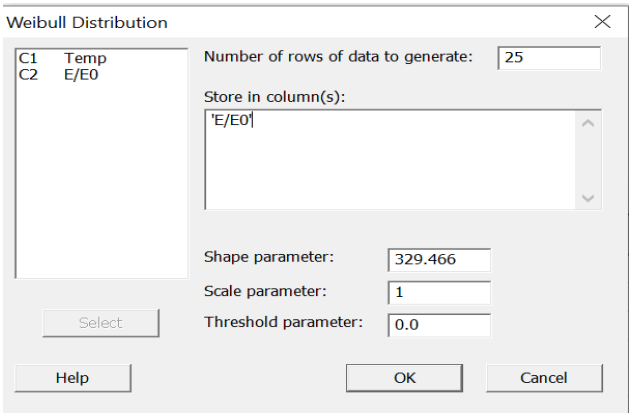

Fig. 10. Generate SRS

The generated results that will be used for the strain analysis simulation are shown in Table 4.

Table 4. SRS Results

Number	Temperature	E/E_0	E
1	190.0300	1.0037	7.9292
2	246.9000	1.0042	7.9333
3	300.7800	1.0040	7.9315
4	393.5900	1.0036	7.9284
5	442.8000	1.0154	8.0216
;			
21	1291.5400	1.2092	9.5525
22	1324.4200	1.2120	9.5752
23	1348.0800	1.2315	9.7285
24	1377.9500	1.2358	9.7631
25	1397.3200	1.2418	9.8099

Fitting was made to the young E/E_0 modulus values at temperatures 400 °C, 600 °C, 800 °C, 1000 °C and 1200 °C for fluences 0 to 6 Zn/cm^2. which were taken from reference data [1] as shown in Figures 11 until 15.

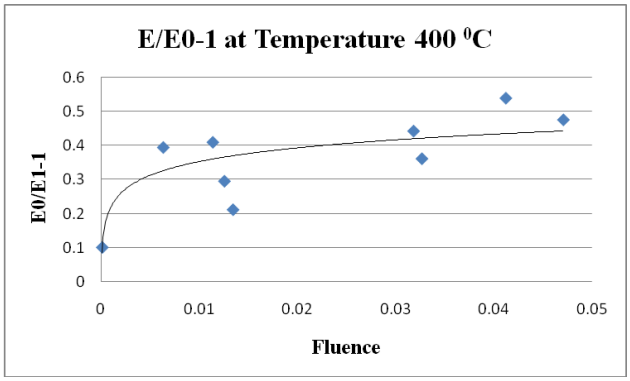

Fig. 11. Normalized Young's modulus change E/ E_0-1 at 400 °C[1]

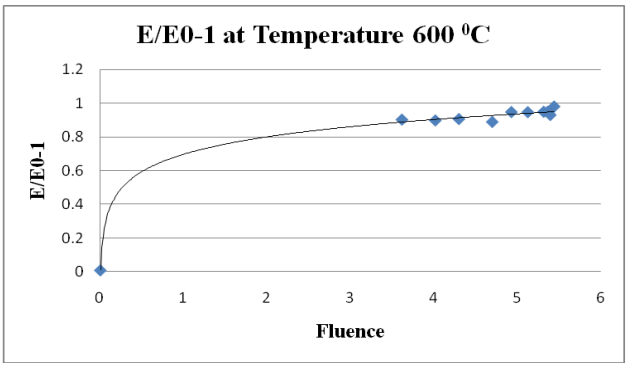

Fig. 12. Normalized Young's modulus change E/ E_0-1 at 600 ℃[1]

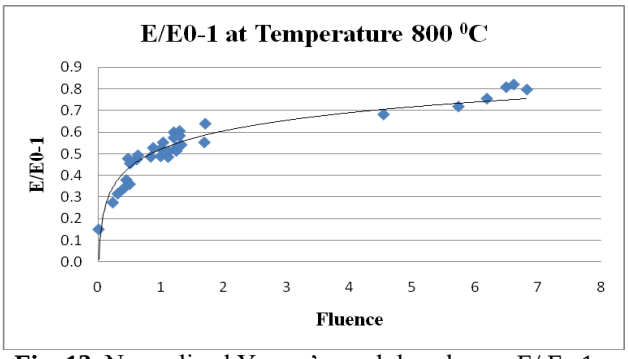

Fig. 13. Normalized Young's modulus change E/ E_0-1 at 800 ℃[1]

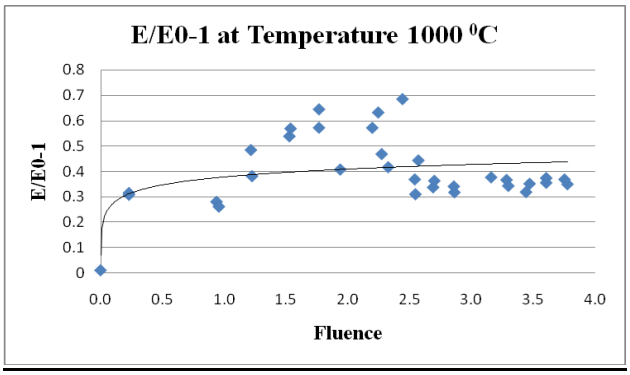

Fig. 14. Normalized Young's modulus change E/ E_0-1 at 1000 °C[1]

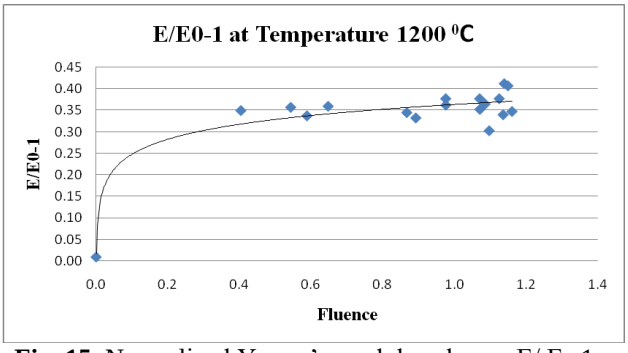

Fig. 15. Normalized Young's modulus change E/ E_0-1 at 1200 °C[1]

The fitting results of the E/E_0-1. The normalized Young's modulus change relative to the Young's modulus at 20 °C, at temperatures of 400 °C, 600 °C, 800 °C, 1000 °C, and 1200 °C were obtained for the experimental results of fluence values shown in Table 5.

Table 5. E/E_0-1 fitting results at fluences < 0.05 Zn/cm^2 and temperature of 400 °C

Fluence (Zn/cm^2)	E/E_0-1	E/E_0	E
0.00631	0.393	1.393	11.00778
0.01136	0.409	1.409	11.12802
0.01254	0.294	1.294	10.22568
0.00342	0.211	1.211	9.563977
0.03181	0.442	1.442	11.38832
0.03266	0.360	1.360	10.74669
0.04121	0.538	1.538	12.15004
0.04707	0.475	1.475	11.64871
0.00631	0.393	1.393	11.00778
0.01136	0.409	1.409	11.12802
0.01254	0.294	1.294	10.22568

A regression model was made from the fitting results for E/E_0-1 at temperatures of 400 °C, 600 °C, 800 °C, 1000 °C, and 1200 °C. Next interpolation was carried out to obtain E/E_0-1 at fluences of 0, 1, 2, 3, 4, 5, and 6 Zn/cm^2 as known in Table 6.

Table 6. E/E_0-1 values for fluence (Zn/cm^2) 0, 1, 2, 3, 4, 5, 6 at temperatures 400 °C, 600 °C, 800 °C, 1000 °C, 1200 °C

Temp	Fluence						
(°C)	0	1	2	3	4	5	6
400	1.28	5.66	10.03	14.4	19	23.15	27.53
600	1.76	1.79	1.83	1.86	1.9	1.93	1.97
800	1.43	1.49	1.55	1.6	1.66	1.72	1.77
1000	1.45	1.43	1.42	1.4	1.39	1.38	1.36
1200	1.33	1.36	1.39	1.42	1.45	1.48	1.51

A regression model was made for E/E_0 for fluences of 0 to 6 Zn/cm^2 at temperatures of 400 °C to 1200 °C. The interpolated values of E/E_0 at temperatures of 600 °C to 800 °C for fluences of 0 to 6 Zn/cm^2 are presented in Table 7.

Table 7. Interpolation results fluence 0, 1, 2, 3, 4, 5, 6 at a temperature of 600°C to 800°C

	Fluence						
Temp	0	1	2	3	4	5	6
600	1.49	1.34	4.88	6.86	8.58	10.26	11.49
610	1.49	1.28	4.76	6.68	8.35	9.96	11.13
620	1.49	1.22	4.64	6.51	8.11	9.67	10.78
630	1.49	1.16	4.52	6.34	7.88	9.38	10.43
650	1.49	1.05	4.30	6.00	7.43	8.81	9.75
665	1.49	0.97	4.13	5.75	7.10	8.40	9.25
680	1.49	0.89	3.97	5.51	6.78	8.00	8.77
700	1.49	0.78	3.76	5.20	6.36	7.48	8.14
725	1.49	0.65	3.51	4.82	5.86	6.85	7.38
740	1.49	0.58	3.36	4.60	5.56	6.48	6.94
750	1.49	0.53	3.26	4.45	5.37	6.24	6.64
765	1.49	0.46	3.12	4.24	5.09	5.88	6.21
775	1.49	0.41	3.02	4.10	4.90	5.65	5.93
790	1.49	0.34	2.88	3.89	4.62	5.30	5.52
800	1.49	0.30	2.79	3.76	4.44	5.08	5.24

The SRS Young's modulus E results are obtained. The minimum, median, average and maximum values of the SRS simulation results dimensional change are shown in Table 8.

Table 8. Minimum, maximum, average and median modulus values of young modulus E for fluence 0, 1, 2, 3, 4, 5, and 6 at temperature around 700 °C

Fluence	E Minimum (MPa)	E Median (MPa)	E Average (MPa)	E Maximum (MPa)
1	1.911.778	6862.447	7408.054	15057.55
2	4136.904	33970.6	40918.2	93275.68
3	6528.755	27733.63	40646.9	109420.5
4	3663.559	22569.8	37755.77	99096.04
5	30283.53	58107.13	55883.68	82966.65
6	26364.66	60397.67	62088.06	101449

Similarly, an SRS simulation was performed for dimensional change values. The stages such as the Young's modulus value, were carried out. The SRS dimensional change results were obtained. The minimum, median, average and maximum values of the SRS simulation results dimensional change are shown in Table 9.

Table 9. Minimum, median, average, maximum values of dimensional changes

Fluence	Minimum (%)	Median (%)	Average (%)	Maximum (%)
0	-0.035	-0.038	-0.554	-2.246
1	-0.125	-1.031	-1.236	-3.75
2	-0.406	-0.908	-0.92	-1.263
3	-0.164	-1.034	-1.42	-3.864
4	-0.188	0.879	-1.42	-10.88
5	-0.202	-1.151	-2.088	-8.205
6	-0.17	-0.878	-1.162	-3.353

A graphite brick, a tenth of the core, is 282 mm wide in the smaller end, 532.3 mm wide in the larger end, 800 mm long, and 300 mm thick. Holes of 130 mm and 80 mm diameters are made as control rod and helium pathways. The graphite component is modeled using Solidworks software package[18]. The design model is shown in Figure 6.

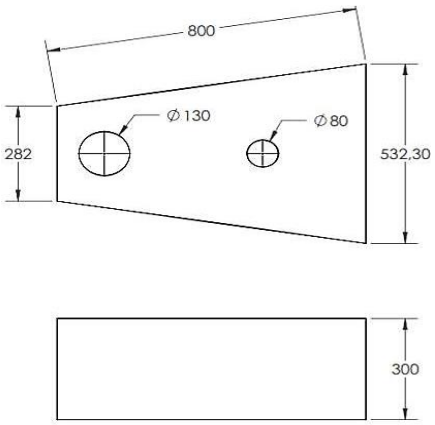

Fig. 16. Size of the Graphite Model

The model needed to be simplified to reduce repeated calculations during simulation. The model was divided into two parts. The simulation model is shown in Figure 17.

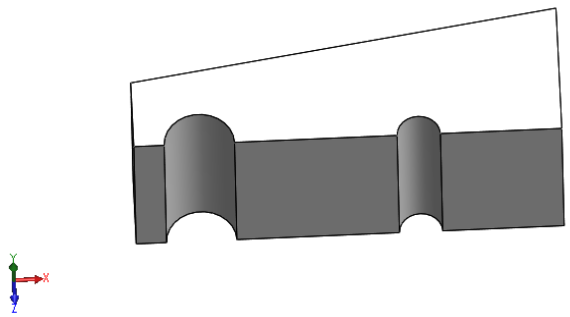

Fig. 17. Simple Graphite Model

The strain distribution simulation is carried out by entering the minimum and maximum values of the Young's modulus and the dimensional change of the SRS results against the model mentioned above. The Young's modulus at room temperature E_0 is 8105.22 MPa obtained by converting the Young's modulus at a temperature of 25 °C to the temperature range of approximately 600 °C to 800 °C.

Simulation of unirradiated and irradiated radial graphite compressive load and load direction is shown in Figure 18.

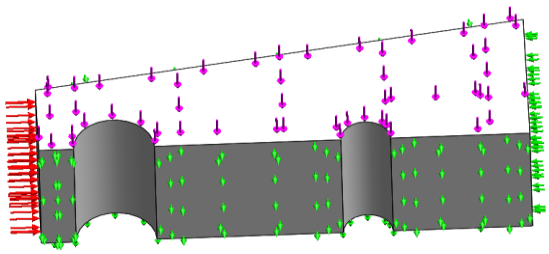

Fig. 18. Direction of a given load

The meshing given to the model is shown in Figure 19.

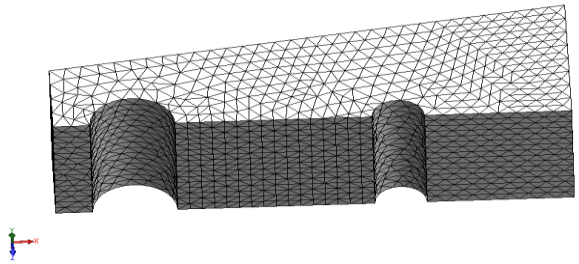

Fig. 19. Meshing model

Meshing is made using the curvature based mesh method with a mesh size of 6.66 - 20 mm. The meshing parameters are stated in Table 10.

Table 10. Mesh Parameters

Mesh type	Solid Mesh
Mesher Used	Curvature-based mesh
Jacobian points	4 points
Max Element Size	25 mm
Min Element Size	8.333 mm
Mesh quality	High
Total nodes	42084
Maximum Aspect Ratio	5.0891
Percentage of elements	
with Aspect Ratio < 3	99.8
with Aspect Ratio > 10	0

The value of the strain distribution or displacement is obtained in graphite material due to its fluence. The displacement values are presented in Table 11. They indicate a dimensional change due to a static load due to the 3-MPa process pressure.

Table 11. Value of graphite displacement due to load

Fluence (10^{21})	Displacement (%)			
	Minimum	Median	Average	Maximum
0	-0.0400	-0.0400	-0.0400	-0.0400
1	-0.1706	-0.0475	-0.0440	-0.0220
2	-0.0788	-0.0096	-0.0079	-0.0035
3	-0.0499	-0.0117	-0.0080	-0.0029
4	-0.0890	-0.0144	-0.0086	-0.0032
5	-0.0107	-0.0002	-0.0058	-0.0039
6	-0.0123	-0.0054	-0.0052	-0.0032

The displacement values show the presence of dimensional change due to static loads due to the 3-MPa process pressure. The displacement distribution is shown in Figure 20.

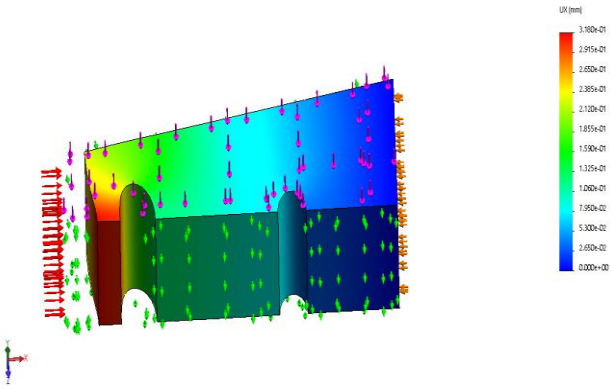

Fig. 20. Distribution of Displacement

The maximum displacement is shown at and near the surface where the process pressure load acts (red section, left).

Figure 21 shows a plot of the dimensional change due to mechanical load to the change in neutron fluence.

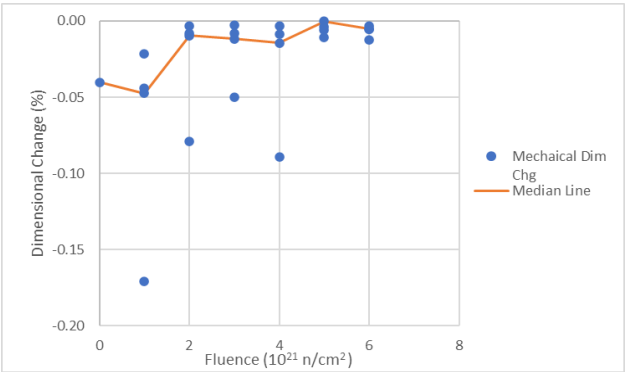

Fig. 21. Plot of dimensional change due to mechanical load to changes in neutron fluence

As seen in Figure 21, as neutron fluence increases the dimensional change value becomes decreasingly negative; the magnitude of dimensional change is getting smaller This is because the modulus of elasticity in the material increases with increasing neutron fluence which

also causes the material to become more brittle. The high modulus of elasticity makes the material difficult to stretch. Figure 22 is a graph showing dimensional changes due to changes in fluence without any external/mechanical loads.

Comparison was made between dimensional changes due to combined fluence and static loads on one hand and dimensional changes due to mechanical loads or external loads alone on the other hand. The difference between the two dimensional changes was determined by comparing Figure 21 and Figure 22.

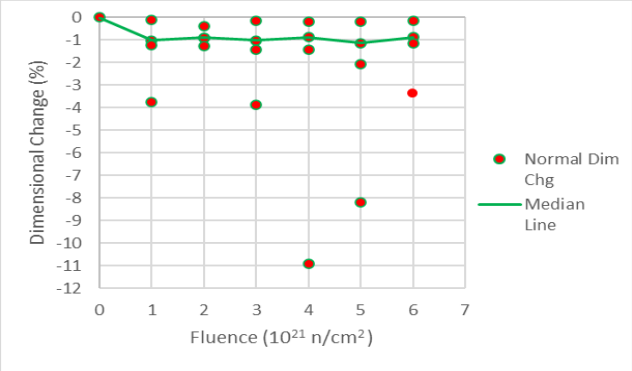

Fig. 22. Plot dimensional change due to changes in fluency without mechanical load

Displacement and strain in the unirradiated model showed higher values compared to the irradiated model. This is because the modulus of elasticity in graphite increases when irradiated. With the irradiation of graphite, the ability of graphite to stretch is reduced or it can be said that graphite is increasingly brittle.

The probabilistic range value changes in graphite IG-110 dimensions due to static loads are shown in Table 12.

Table 12. Value ranges due to static load

Neutron Fluence	Dimensional Change (%)
0	-0.0400
1	-0.1706 < D < -0.0220
2	-0.0788 <D < -0.0035
3	-0.0499 < D < -0.0029
4	-0.0890 < D < -0.0032
5	-0.0107 < D < -0.0039
6	-0.0123 < D < -0.0032

5. CONCLUSION

The stress analysis method has been tested using a probabilistic method based on simple random sampling. The probabilistic analysis method can be used to provide the distribution of stress analysis values within the reflector due to the distribution generated by the mechanical properties of the IG-110 graphite material. Simulations were carried out using SolidWorks based on finite element method. Deformation of the reflector component made of IG-110 in the HTGR reactor occurs due to mechanical loads temperature differences when operating and neutron fluence. Of the three causes of deformation mechanical loads has the greatest influence.

ACKNOWLEDGMENT

The author would like to acknowledge RISTEK who has supported this research. This research is funded by FLAGSHIP PTKRN BATAN 2019.

AUTHOR CONTRIBUTION

Mike Susmikanti, Roziq Himawan, Farisy Yogatama Sulistyo and Jos Budi Sulistyo equally contributed as the main contributors of this paper. All authors read and approved the final version of the paper.

REFERENCES

1. Himawan R., Sudadiyo S., Saragi E. Comparison Study on Model of Creep Strain for Graphite Material at HTGR. Prosiding Seminar Nasional Teknologi Energi Nuklir. 2016. 385-392.
2. Liu D., Mingard K., Lord O.T., Flewitt P. On the Damage and Fracture of Nuclear Graphite at Multiple Length-scales. J. Nucl. Mater. 2017. **493**:246-254.
3. Heijna M.C.R., de Groot S., Vreeling J.A. Comparison of Irradiation Behaviour of HTR Graphite Grades. J. Nucl. Mater. 2017. **492**:148-156.
4. Tian D., Shi L., Sun L., Zhang Z., Zhang Z., Zhang Z. Installation of the Graphite Internals in HTR-PM. Nucl. Eng. Des. 2020. **363**:1-10.
5. Xu Y., Li H., Xie F., Cao J., Tong J. Source Term Analysis of Tritium in HTR-10. Fusion Sci. Technol. 2017. **71**(4):671-678.
6. Wankui Y., Songbao Z., Yaoguang L., Weili N., Li D. Neutron Fluence Analysis of Graphite Reflector in SPRR-300 during the Whole Reactor Lifetime. Ann. Nucl. Energy. 2017. **106**:91-96.
7. He X., Shi L., Li H., Tan J., Zhang B., Fok A., et al. Experimental Study to Estimate the Surface Wear of Wuclear Graphite in HTR-PM. Ann. Nucl. Energy. 2018. **116**:296-302.
8. Himawan R., Lie F., Dewi Basoeki P.,

Haryanto M. Applicability Study of Ultrasonic Flaw Detector For Nuclear Grade Graphite Examination. J. Phys. Conf. Ser. 2019. **1198**:1-8.

9. Li Z. Sen, Tang L.S. Using Synchrotron-Based X-Ray Microcomputed Tomography to Characterize Water Distribution in Compacted Soils. Adv. Mater. Sci. Eng. 2019. **2019**:1-12.
10. Himawan R., Sutrasno, Santoso S.B. Non-destructive Evaluation of Nuclear Grade IG-110 Graphite Using Constant Potential X-Ray. J. Phys. Conf. Ser. 2020. **1436**:1-7.
11. Hartini E., Himawan R., Susmikanti M. Fracture Mechanics Uncertainty Analysis in the Reliability Assessment of the Reactor Pressure Vessel: (2D) Subjected To Internal Pressure. J. Teknol. Reakt. Nukl. Tri Dasa Mega. 2016. **18**(2):55-64.
12. Susmikanti M., Himawan R., Hafid A., Hartini E. Evaluation on Mechanical Fracture of PWR Pressure Vessel and Modeling Based on Neural Network. J. Teknol. Reakt. Nukl. Tri Dasa Mega. 2016. **18**(2):87-100.
13. Hashim A., Kyaw S., Sun W. Modelling Fracture of Aged Graphite Bricks under Radiation and Temperature. Nucl. Mater. Energy. 2017. **11**:3-11.
14. Hartini E., Himawan R., Susmikanti M. Analisis Probabilistic Fracture Mechanics Pada Evaluasi Keandalan Bejana Tekan Reaktor Secara 3-D. Urania J. Ilm. Daur Bahan Bakar Nukl. 2018. **24**(1):51-60.
15. Bobba S., Abrar S., Rehman S.M. Probability Study on the Thermal Stress Distribution in Thick hk40 Stainless Steel Pipe using Finite Element Method. Designs. 2019. **3**(1):1-26.
16. Susmikanti M., Hartini E., Saepudin A., Sulistyo J.B. Component Analysis of Purification System of RSG-GAS. J. Pengemb. Energi Nukl. 2018. **20**(1):31-39.
17. Hao C., Li P., She D., Zhou X., Yang R. Sensitivity and Uncertainty Analysis of the Maximum Fuel Temperature under Accident Condition of HTR-PM. Sci. Technol. Nucl. Install. 2020. **2020**:1-21.
18. Hong C.C., Chang C.L., Lin C.Y. Static Structural Analysis of Great Five-axis Turning-milling Complex CNC Machine. Eng. Sci. Technol. an Int. J. 2016. **19**(4):71-84.